Electromagnetic Scattering Model for a Tree Trunk Above a Tilted Ground Plane

Yi-Cheng Lin, *Student Member, IEEE*, and Kamal Sarabandi, *Senior Member, IEEE*

Abstract—**An efficient and realistic electromagnetic scattering model for a tree trunk above a ground plane is presented in this paper. The trunk is modeled as a finite-length stratified dielectric cylinder with a corrugated bark layer. The ground is considered to be a smooth homogeneous dielectric with an arbitrary slope. The bistatic scattering response of the cylinder is obtained by invoking two approximations. In the microwave region, the height of the tree trunks are usually much larger than the wavelength. Therefore the interior fields in a finite length cylinder representing a tree trunk can be approximated with those of an infinite cylinder with the same physical and electrical radial characteristics. Also an approximate image theory is used to account for the presence of the dielectric ground plane which simply introduces an image excitation wave and an image scattered field. An asymptotic solution based on the physical optics approximation is derived which provides a fast algorithm with excellent accuracy when the radii of the tree trunks are large compared to the wavelength. The effect of a bark layer is also taken into account by simply replacing the bark layer with an anisotropic layer. It is shown that the corrugated layer acts as an impedance transformer which may significantly decrease the backscattering radar cross section depending on the corrugation parameters. It is also shown that for a tilted ground plane a significant cross-polarized backscattered signal is generated while the co-polarized backscattered signal is reduced.**

I. Introduction

BECAUSE of the important role of the earth's vegetation cover on climatic changes, characterization of physical parameters of the vegetation cover remotely and globally is of great importance. In recent years, considerable effort has been devoted to the development of electromagnetic scattering models for forest canopy [1]–[3]. In these models the forest canopy is considered to be composed of simple geometrical particles having different sizes, shapes, and dielectric constants. Using vector radiative transfer theory, it has been shown that the backscattering from a typical forest stand can be decomposed into four scattering components: 1) direct backscattering from the crown layer, 2) bistatic scattering from the crown layer reflected from the ground plane, 3) bistatic scattering from the trunk layer reflected from the ground plane, 4) direct backscattering from the ground plane [1]. In lower microwave frequency and/or when the crown layer is tenuous the backscattering is dominated by the ground-trunk interaction. Therefore the accuracy of the scattering model in such cases is directly proportional to the accuracy of the scattering model for tree trunks above a ground plane.

In the mentioned models of forest stands, a tree trunk is simply modeled by a vertical, homogeneous, finite-length dielectric cylinder. The scattering solutions for a finite-length cylinder, reported in the literature, are either based on the eigen-function expansion solution for an infinite cylinder [1]–[5], or low frequency approximation where all dimensions of the cylinder are small compared to the wavelength [6]. When the cylinder radius is large compared to the wavelength the eigen-function solution becomes, numerically, inefficient due to the poor rate of convergence of the series involved in the solution. This is the case in the microwave region where the radius of tree trunks in a forest stand can be significantly larger than the wavelength. An inefficient solution for the calculation of scattering properties of a canopy constituent particles makes the canopy model numerically intractable because the scattering solution for individual particles must be evaluated many times to account for the particle variability in size and orientation. Moreover, in modeling a tree trunk with a dielectric cylinder, an important feature of the tree trunk, the bark layer, has been overlooked. For many trees, the bark layer is rough and can be represented by longitudinal grooves on the surface of a dielectric cylinder having possibly a different dielectric constant. The effect of the bark layer on the RCS of a tree trunk was demonstrated recently by representing the bark layer with a corrugated dielectric layer [7]. Using a hybrid scattering model based on the method of moments and physical optics it was shown that the RCS of a tree trunk is significantly reduced when the effect of the bark layer is taken into account. However this model is not numerically efficient enough to be used in conjunction with the scattering model for a forest canopy.

In this paper, a realistic and efficient scattering model for a tree trunk above a ground plane is developed. In this model the effect of the radial inhomogeneity as well as the rough bark layer are taken into consideration. Relying on the fact that the dielectric constants of tree trunks are highly lossy, the physical optics (PO) approximation is used at high frequencies where the radius of curvature is large compared to the wavelength. For finite-length cylinders having radii comparable to the wavelength, the eigen-function expansion in conjunction with the field equivalence principle is used. The bark layer is represented by a periodic corrugated layer

Manuscript received June 17, 1994; revised Jan. 31, 1995.

The authors are with the Radiation Laboratory, Department of Electrical Engineering and Computer Science, University of Michigan, Ann Arbor, MI 48109-2122 USA.

IEEE Log Number 9412805.

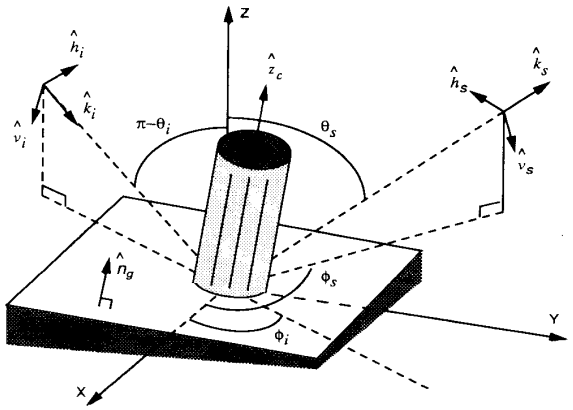

Fig. 1. Global coordinate system.

and equivalently replaced by an anisotropic layer as suggested in [9]. The ground plane is considered to be a homogeneous medium having a smooth interface and both the cylinder and the ground plane are allowed to have arbitrary orientation with respect to the global coordinate system. Numerical simulations are demonstrated in Section VII where the region of validity of the PO approximation and the effect of a bark layer and a tilted ground plane are investigated.

II. Global Coordinate System

In this paper, the problem of scattering from a cylinder above a ground plane in the most general configuration is considered as shown in Fig. 1. A global coordinate system (X, Y, Z) is constructed to describe the directional vector $\hat{u}$,

$$\hat{u}(\theta, \phi) = \hat{X} \sin\theta \cos\phi + \hat{Y} \sin\theta \sin\phi + \hat{Z} \cos\theta \quad (1)$$

representing the unit vector along the incidence direction $\hat{k}_i(\theta_i, \phi_i)$, the scattering direction $\hat{k}_s(\theta_s, \phi_s)$, the orientation direction of the cylinder $\hat{z}_c(\theta_c, \phi_c)$, or the unit normal to the ground plane $\hat{n}_g(\theta_g, \phi_g)$. In this coordinate system, the horizontal and vertical polarization of the incident and the scattered waves are defined by

$$\hat{h}_p = \hat{Z} \times \hat{k}_p / |\hat{Z} \times \hat{k}_p| \quad (2)$$

$$\hat{v}_p = \hat{h}_p \times \hat{k}_p \quad (3)$$

where subscript p can be i or s. In this paper, the forward scatter alignment convention [6] will be used. The components of the scattered field $\mathbf{E}^s$ and the incident field $\mathbf{E}^i$ in the global coordinate system can be related to each other by the scattering matrix $\mathbf{S}$, i.e.,

$$\begin{pmatrix} E_v^s \\ E_h^s \end{pmatrix} = \frac{e^{ik_o r}}{r} \begin{pmatrix} S_{vv} & S_{vh} \\ S_{hv} & S_{hh} \end{pmatrix} \begin{pmatrix} E_v^i \\ E_h^i \end{pmatrix}. \quad (4)$$

The ground is assumed to be smooth having an arbitrary slope in the global coordinate system. It can be shown [8] that when the observation point is away from the ground plane interface and in the far field region of the scatterer, the effect of the ground plane on scattering can simply be taken into account by including the mirror image contributions. Hence the scattering matrix consists only of four components,

$$\mathbf{S} = \mathbf{S}_t + \mathbf{S}_{gt} + \mathbf{S}_{tg} + \mathbf{S}_{gtg} \quad (5)$$

where

$$\mathbf{S}_t = \mathbf{S}^0(\hat{k}_s, \hat{k}_i) \quad (6)$$

$$\mathbf{S}_{gt} = e^{i\tau_s} \boldsymbol{\Gamma}(\hat{k}_s, \hat{n}_g, \hat{k}_{sg}) \cdot \mathbf{S}^0(\hat{k}_{sg}, \hat{k}_i) \quad (7)$$

$$\mathbf{S}_{tg} = e^{i\tau_i} \mathbf{S}^0(\hat{k}_s, \hat{k}_{gi}) \cdot \boldsymbol{\Gamma}(\hat{k}_{gi}, \hat{n}_g, \hat{k}_i) \quad (8)$$

$$\mathbf{S}_{gtg} = e^{i(\tau_i+\tau_s)} \boldsymbol{\Gamma}(\hat{k}_s, \hat{n}_g, \hat{k}_{sg}) \cdot \mathbf{S}^0(\hat{k}_{sg}, \hat{k}_{gi}) \cdot \boldsymbol{\Gamma}(\hat{k}_{gi}, \hat{n}_g, \hat{k}_i). \quad (9)$$

Here,

$$\hat{k}_{gi} = \hat{k}_i - 2\hat{n}_g(\hat{n}_g \cdot \hat{k}_i)$$

$$\hat{k}_{sg} = \hat{k}_s - 2\hat{n}_g(\hat{n}_g \cdot \hat{k}_s)$$

$$\tau_i = -k_0 b(\hat{n}_g \cdot \hat{z}_c)(\hat{n}_g \cdot \hat{k}_i)$$

$$\tau_s = k_0 b(\hat{n}_g \cdot \hat{z}_c)(\hat{n}_g \cdot \hat{k}_s).$$

In the approximation (5) higher order scattering terms, such as multiple scattering between the object and its mirror image, have been ignored. In the above expressions, the optical lengths τ_i and τ_s account for the extra path lengths of the image excitation and the image scattered waves respectively. $\mathbf{S}^0(\hat{k}_s, \hat{k}_i)$ is the scattering matrix of the isolated target in free space, and $\boldsymbol{\Gamma}(\hat{k}_r, \hat{n}_g, \hat{k}_i)$ is the reflection matrix which accounts for the specular reflection and polarization transformation due to the tilted ground plane. In order to provide a physical insight for each term in (6)–(9), subscripts t and g are added to represent the scattering from the trunk and the reflection from the ground plane respectively. The order of the subscripts indicates the sequence of scattering in the first order solution. The unit vectors indicating the direction of incident, scattered, and reflected waves, as shown in Fig. 1, are also expressed in the arguments of $\mathbf{S}^0$ and $\boldsymbol{\Gamma}$ in the same order. In most cases the total backscattered signal is dominated by the specular terms $\mathbf{S}_{gt}$ and $\mathbf{S}_{tg}$.

In the following sections, a general reflection matrix $\boldsymbol{\Gamma}$ for a tilted ground plane with arbitrary slope is first obtained, and then the bistatic expressions for the scattering matrix $\mathbf{S}^0$ of a stratified finite cylinder in free space based on the eigenfunction expansion and the PO approximation are derived.

III. Reflection Coefficient Matrix for a Tilted Ground Plane

In most scattering models for forest stands, the effect of the surface topography is ignored. Reference [10] showed the importance of the ground tilt angle in the radar backscatter. In this section, an expression for the reflection matrix of a tilted ground plane is derived which will be used to develop a polarimetric scattering formulation for a cylinder with arbitrary orientation above a tilted ground plane.

Consider a tilted ground plane with a unit normal $\hat{n}_g(\theta_g, \phi_g)$ that is illuminated by a plane wave propagating in $\hat{k}_i$ direction. The direction of the reflected wave is given by

$$\hat{k}_r = \hat{k}_i - 2\hat{n}_g(\hat{n}_g \cdot \hat{k}_i) \tag{10}$$

which is normal to $\mathbf{E}^r$ having E_v^r and E_h^r as its vertical and horizontal components in the global coordinate system. Defining the reflection coefficient matrix $\mathbf{\Gamma}$ by

$$\mathbf{E}^r = \boldsymbol{\Gamma}(\hat{k}_r, \hat{n}_g, \hat{k}_i) \cdot \mathbf{E}^i \tag{11}$$

the objective is to express the elements of $\mathbf{\Gamma}$ in terms of the Fresnel reflection coefficients of the ground plane. In the local coordinate of the ground plane, the vertical and horizontal polarization of a wave are defined by

$$\hat{h}'_p = \hat{n}_g \times \hat{k}_p / |\hat{n}_g \times \hat{k}_p| \tag{12}$$

$$\hat{v}'_p = \hat{h}'_p \times \hat{k}_p \tag{13}$$

where the subscript p can be i or r. By representing both the incident and reflected field vectors in the local coordinate system $(\hat{v}'_p, \hat{h}'_p, \hat{k}_p)$ and noting that

$$\begin{pmatrix} E^r_{v'} \\ E^r_{h'} \end{pmatrix} = \begin{pmatrix} \Gamma_{v'} & 0 \\ 0 & \Gamma_{h'} \end{pmatrix} \begin{pmatrix} E^i_{v'} \\ E^i_{h'} \end{pmatrix} \tag{14}$$

the elements of the reflection coefficient matrix can be obtained from

$$\Gamma_{pq} = (\hat{p}_r \cdot \hat{v}'_r)\Gamma_{v'}(\hat{v}'_i \cdot \hat{q}_i) + (\hat{p}_r \cdot \hat{h}'_r)\Gamma_{h'}(\hat{h}'_i \cdot \hat{q}_i) \tag{15}$$

where p and q can be v or h, and $\Gamma_{v'}$ and $\Gamma_{h'}$ are, respectively, the vertical and horizontal Fresnel reflection coefficients of the ground plane. The inner products in the above expression in terms of the global coordinate parameters are given by

$$\begin{aligned} \hat{v}_j \cdot \hat{v}'_j &= \hat{h}_j \cdot \hat{h}'_j \\ &= \frac{\hat{n}_g \cdot \hat{Z} - (\hat{k}_j \cdot \hat{Z})(\hat{n}_g \cdot \hat{k}_j)}{|\hat{n}_g \times \hat{k}_j|\,|\hat{Z} \times \hat{k}_j|} \\ \hat{v}_j \cdot \hat{h}'_j &= -\hat{h}_j \cdot \hat{v}'_j \\ &= \frac{\hat{n}_g \cdot \hat{h}_j}{|\hat{n}_g \times \hat{k}_j|} \end{aligned}$$

where j can be i or r.

The local slope has two significant effects on the backscatterer: 1) depending on the slope angle and the trunk height, the ground-trunk term in the backscattering direction reduces, and 2) a significant cross-polarized component is generated through the reflection from the slanted ground plane which enhances the cross-polarized backscattering coefficient. These two effects will be examined and illustrated later.

IV. A Semiexact Solution

Scattered fields of an infinite stratified cylinder can be obtained by the standard eigen-function expansion method [11]. However, for finite-length cylinders, no exact solution exists. In the microwave region where the length of a tree trunk is much larger than the wavelength and the dielectric constant has a significant imaginary part, the effect of the longitudinal traveling waves on a finite cylinder can be ignored. Therefore, the internal fields of a finite cylinder may be approximated by those of an infinite cylinder having the same radial characteristics. In this paper the scattered fields of a finite cylinder is obtained by invoking the field equivalence principle. That is the dielectric cylinder is replaced by fictitious electric and magnetic surface currents $\mathbf{J}$ and $\mathbf{M}$ given by

$$\mathbf{J} = \hat{n} \times \mathbf{H} \tag{16}$$

$$\mathbf{M} = -\hat{n} \times \mathbf{E} \tag{17}$$

where $\mathbf{H}$ and $\mathbf{E}$ are the total (incident plus scattered) magnetic and electric fields on the surface of the cylinder, and $\hat{n}$ is the unit vector outward normal to the cylinder surface. These fields are approximated by those of the infinite cylinder, and their tangential components on the surface of the cylinder are given by

$$E_z(\rho' = a, \phi', z') = \sum_n E_{zn} e^{i(\hat{k}_i \cdot \hat{z}' z' + n\phi')} \tag{18}$$

$$Z_0 H_z(\rho' = a, \phi', z') = \sum_n H_{zn} e^{i(\hat{k}_i \cdot \hat{z}' z' + n\phi')} \tag{19}$$

$$E_\phi(\rho' = a, \phi', z') = \sum_n E_{\phi n} e^{i(\hat{k}_i \cdot \hat{z}' z' + n\phi')} \tag{20}$$

$$Z_0 H_\phi(\rho' = a, \phi', z') = \sum_n H_{\phi' n} e^{i(\hat{k}_i \cdot \hat{z}' z' + n\phi')} \tag{21}$$

where Z_0 is the intrinsic impedance of the free space and E_{zn}, H_{zn}, $E_{\phi n}$, and $H_{\phi n}$ are the Fourier components of electric and magnetic field which can be found in a recursive fashion for a stratified cylinder as shown in [12]. In (18)–(21), (ρ', ϕ', z') define a local coordinate system in which the cylinder axis $\hat{z}_c$ is along $\hat{z}'$ and $\hat{y}' = (\hat{k}_i \times \hat{z}')/|\hat{k}_i \times \hat{z}'|$. Using the fictitious current sources, the electric and magnetic Hertz vector potentials can be evaluated from

$$\begin{aligned} \boldsymbol{\Pi}_e(\bar{r}) = \frac{iZ_0}{4\pi k_0} \frac{e^{ik_o r}}{r} \int_{-b/2}^{b/2} \int_0^{2\pi} \\ \cdot \mathbf{J}(z', \phi') e^{-ik_0 \hat{k}_s \cdot \bar{r}'} a\, d\phi'\, dz' \end{aligned} \tag{22}$$

$$\begin{aligned} \boldsymbol{\Pi}_m(\bar{r}) = \frac{iY_0}{4\pi k_0} \frac{e^{ik_o r}}{r} \int_{-b/2}^{b/2} \int_0^{2\pi} \\ \cdot \mathbf{M}(z', \phi') e^{-ik_0 \hat{k}_s \cdot \bar{r}'} a\, d\phi'\, dz'. \end{aligned} \tag{23}$$

where b is the height of the cylinder. The scattered field in the radiation zone (far field region) of the cylinder can be obtained from

$$\mathbf{E}^s = -k_0^2[\hat{k}_s \times (\hat{k}_s \times \boldsymbol{\Pi}_e) + \hat{k}_s \times (Z_0 \boldsymbol{\Pi}_m)]. \tag{24}$$

After some algebraic manipulation as shown in [14], the elements of the scattering matrix for the finite-length cylinder

in free space are found to be

$$S_{vv}^0 = -\frac{iab}{4\pi k_0}\frac{\sin V}{V}\left[(\hat{v}_s\cdot\hat{z}')I(\hat{v}_i)+(\hat{h}_s\cdot\hat{z}')K(\hat{v}_i)\right] \quad (25)$$

$$S_{vh}^0 = -\frac{iab}{4\pi k_0}\frac{\sin V}{V}\left[(\hat{v}_s\cdot\hat{z}')I(\hat{h}_i)+(\hat{h}_s\cdot\hat{z}')K(\hat{h}_i)\right] \quad (26)$$

$$S_{hv}^0 = -\frac{iab}{4\pi k_0}\frac{\sin V}{V}\left[(\hat{h}_s\cdot\hat{z}')I(\hat{v}_i)-(\hat{v}_s\cdot\hat{z}')K(\hat{v}_i)\right] \quad (27)$$

$$S_{hh}^0 = -\frac{iab}{4\pi k_0}\frac{\sin V}{V}\left[(\hat{h}_s\cdot\hat{z}')I(\hat{h}_i)-(\hat{v}_s\cdot\hat{z}')K(\hat{h}_i)\right] \quad (28)$$

where

$$I = \sum_n \left\{ H_{\phi n}u_{1n} + \frac{\hat{k}_s\cdot\hat{z}'}{B} \cdot(\sin\tilde{\phi}H_{zn}u_{2n} - \cos\tilde{\phi}H_{zn}u_{1n}) - \frac{\sin\tilde{\phi}}{B}E_{zn}u_{3n} - \frac{\cos\tilde{\phi}}{B}E_{zn}u_{2n}\right\} \quad (29)$$

$$K = -\sum_n \left\{ E_{\phi n}u_{1n} + \frac{\hat{k}_s\cdot\hat{z}'}{B} \cdot(\sin\tilde{\phi}E_{zn}u_{2n} - \cos\tilde{\phi}E_{zn}u_{3n}) - \frac{\sin\tilde{\phi}}{B}H_{zn}u_{3n} - \frac{\cos\tilde{\phi}}{B}H_{zn}u_{2n}\right\} \quad (30)$$

with

$$V = \frac{k_0 b}{2}(\hat{k}_i - \hat{k}_s)\cdot\hat{z}'$$

$$u_{1n} = 2\pi(-i)^n J_n(y_0)e^{in\tilde{\phi}}$$

$$u_{2n} = 2\pi(-i)^n\left\{i\cos\tilde{\phi}J_n'(y_0) + \sin\tilde{\phi}\frac{n}{y_0}J_n(y_0)\right\}e^{in\tilde{\phi}}$$

$$u_{3n} = 2\pi(-i)^n\left\{i\sin\tilde{\phi}J_n'(y_0) - \cos\tilde{\phi}\frac{n}{y_0}J_n(y_0)\right\}e^{in\tilde{\phi}}$$

$$B = \sqrt{(\hat{k}_s\cdot\hat{x}')^2 + (\hat{k}_s\cdot\hat{y}')^2}$$

$$\tilde{\phi} = \tan^{-1}\left(\frac{\hat{k}_s\cdot\hat{y}'}{\hat{k}_s\cdot\hat{x}'}\right)$$

$$y_0 = k_0 aB. \quad (31)$$

Here J_n and J_n' are, respectively, the Bessel function of first kind and its derivative. It should be noted that I and K as given by (29) and (30) are functions of the polarization of the incident wave.

V. Physical Optics Approximation

The semi-exact solution described in the previous section becomes inefficient at high frequencies where the radius of the cylinder is large compared to the wavelength and fails when the cross section of the cylinder is not circular. These deficiencies can be removed at high frequencies by employing the PO approximation. This approximation is valid when the radius of curvature of the cylinder is large compared to the wavelength and the permittivity of the cylinder has a relatively large imaginary part so that the effect of the glory rays and the creeping waves could be ignored. As before, the cylinder is replaced by fictitious electric and magnetic currents, however in this case, the currents are approximated by those of the local tangential plane which are proportional to the sum of the incident and reflected waves.

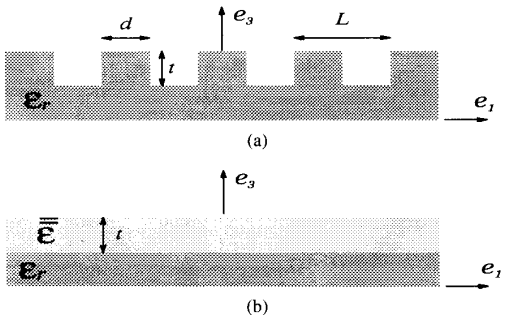

Fig. 2. (a) A corrugated layer and (b) its equivalent anisotropic layer.

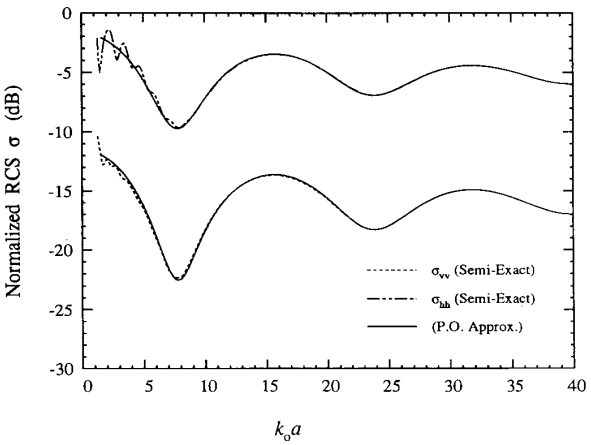

Fig. 3. Comparison of the PO approximation with the semi-exact solution. The ratio of the interior radius a_2 and the exterior radius $a_1(=a)$ is kept constant $(a_2/a_1 = 0.9)$. Other parameters are $b = 20\lambda_0$, $\epsilon_1 = 4 + i1$, $\epsilon_2 = \epsilon_g = 10 + i5$, $\theta_i = 120°$, $\phi_i = 180°$, $\theta_s = 60°$, $\phi_s = 0°$, $\theta_g = \theta_c = 0°$.

To simplify the integration of the currents over the lit surface, the stationary phase (SP) approximation may be used. This approximation is valid so long as the stationary point falls over the lit region. For convenience, a local coordinate $(\hat{n}, \hat{t}, \hat{l})$ is established at the SP point. The local tangential directions are defined by

$$\hat{t} = \hat{n}\times\hat{k}_i/|\hat{n}\times\hat{k}_i| \quad (32)$$

$$\hat{l} = \hat{n}\times\hat{t} \quad (33)$$

where $\hat{n}$ is a unit vector normal to the cylinder surface at the SP point. For the general case of an anisotropic medium (the bark layer may exhibit anisotropic properties) a dyadic reflection coefficient $\mathbf{R}$ is introduced to relate the polarization coupling between the incident and reflected waves, i.e.,

$$\mathbf{E}_T^r = \mathbf{R}\cdot\mathbf{E}_T^i. \quad (34)$$

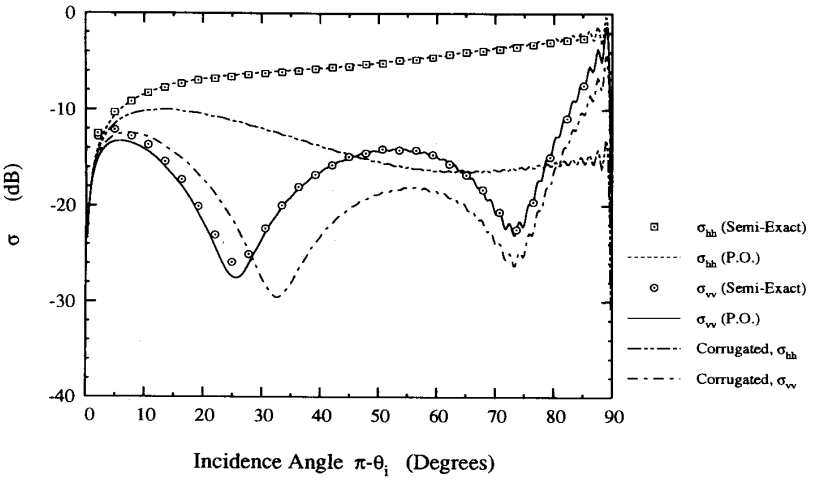

Fig. 4. The normalized backscattering RCS as a function of the incidence angle $\theta = \pi - \theta_i$ for a two layered cylinder with and without the corrugation. Other parameters are $b = 20\lambda_0$, $a_1 = 2\lambda_0$, $a_2 = 1.8\lambda$, $t = 0.1\lambda_0$, $d/L = 0.7$, $\phi_i = 180°$, $\phi_s = 0°$, $\theta_g = \theta_c = 0°$.

Combining the incident and reflected fields, the total fields $\mathbf{E}(= \mathbf{E}^r + \mathbf{E}^i)$ and $\mathbf{H}(= \mathbf{H}^r + \mathbf{H}^i)$ on the surface of the cylinder can be obtained from

$$\begin{pmatrix} E_l \\ E_t \end{pmatrix} = \begin{pmatrix} 1 + R_{vv} & R_{vh} \\ R_{hv} & 1 + R_{hh} \end{pmatrix} \begin{pmatrix} E_l^i \\ E_t^i \end{pmatrix} \tag{35}$$

and

$$\begin{pmatrix} H_l \\ H_t \end{pmatrix} = \begin{pmatrix} 1 - R_{hh} & R_{hv} \\ R_{vh} & 1 - R_{vv} \end{pmatrix} \begin{pmatrix} H_l^i \\ H_t^i \end{pmatrix}. \tag{36}$$

Applying the stationary phase approximation, it can be shown that the Hertz vector potentials are given by

$$\Pi_e = \frac{iZ_0}{k_0} \frac{e^{ik_o r}}{r} Q\mathbf{J} \tag{37}$$

$$\Pi_m = \frac{iY_0}{k_0} \frac{e^{ik_o r}}{r} Q\mathbf{M} \tag{38}$$

where $\mathbf{J}$ and $\mathbf{M}$ are the fictitious currents evaluated from the total fields $\mathbf{E}$ and $\mathbf{H}$ at the SP point ($\phi' = \tilde{\phi}$), and

$$\begin{aligned} Q &= \frac{ik_0}{4\pi} \int_{-b/2}^{b/2} \int_{-\pi/2}^{\pi/2} \\ &\quad \cdot e^{-ik_0 aB \cos(\phi' - \tilde{\phi})} e^{ik_0(\hat{k}_i - \hat{k}_s)\cdot \hat{z} z'} a \, d\phi' \, dz' \\ &= \frac{ib}{2\pi} \frac{\sin V}{V} e^{-ik_0 Ba} \sqrt{\frac{k_0 a}{2B}} \\ &\quad \cdot \left\{ F\left[\sqrt{\frac{k_0 Ba}{2}} \left(\frac{\pi}{2} + \tilde{\phi} \right) \right] \right. \\ &\quad \left. + F\left[\sqrt{\frac{k_0 Ba}{2}} \left(\frac{\pi}{2} - \tilde{\phi} \right) \right] \right\} \end{aligned} \tag{39}$$

with

$$B = \{ [(\hat{k}_s - \hat{k}_i) \cdot \hat{x}']^2 + [(\hat{k}_s - \hat{k}_i) \cdot \hat{y}']^2 \}^{1/2}$$

$$\tilde{\phi} = \tan^{-1} \left[\frac{(\hat{k}_s - \hat{k}_i) \cdot \hat{y}'}{(\hat{k}_s - \hat{k}_i) \cdot \hat{x}'} \right]$$

and $F(\cdot)$ is the Fresnel Integral. This approximation is valid provided $k_0 aB \gg 1$ and $\tilde{\phi}$ is away from the shadow boundary.

Using a similar procedure as in the previous section, the scattering matrix elements are found to be

$$\begin{aligned} S_{vv}^0 &= Q[(\hat{l} \cdot \hat{v}_s) Z_0 J_{lv} + (\hat{t} \cdot \hat{v}_s) Z_0 J_{tv} \\ &\quad + (\hat{l} \cdot \hat{h}_s) M_{lv} + (\hat{t} \cdot \hat{h}_s) M_{tv}] \end{aligned} \tag{40a}$$

$$\begin{aligned} S_{vh}^0 &= Q[(\hat{l} \cdot \hat{v}_s) Z_0 J_{lh} + (\hat{t} \cdot \hat{v}_s) Z_0 J_{th} \\ &\quad + (\hat{l} \cdot \hat{h}_s) M_{lh} + (\hat{t} \cdot \hat{h}_s) M_{th}] \end{aligned} \tag{40b}$$

$$\begin{aligned} S_{hv}^0 &= Q[(\hat{l} \cdot \hat{h}_s) Z_0 J_{lv} + (\hat{t} \cdot \hat{h}_s) Z_0 J_{tv} \\ &\quad - (\hat{l} \cdot \hat{v}_s) M_{lv} - (\hat{t} \cdot \hat{v}_s) M_{tv}] \end{aligned} \tag{40c}$$

$$\begin{aligned} S_{hh}^0 &= Q[(\hat{l} \cdot \hat{h}_s) Z_0 J_{lh} + (\hat{t} \cdot \hat{h}_s) Z_0 J_{th} \\ &\quad - (\hat{l} \cdot \hat{v}_s) M_{lh} - (\hat{t} \cdot \hat{v}_s) M_{th}] \end{aligned} \tag{40d}$$

where J_{pq} and M_{pq} are the currents along $\hat{p}$ direction induced by a $\hat{q}$ polarized incident wave (p can be t or l and q can be v or h). The inner products of the vectors in the above expressions can easily be calculated in terms of the global coordinates.

The above results fail in the case of forward scattering for which $B = 0$. However, in directions close to the forward direction, an alternative approximation for the scattered field is possible and is given by [14]

$$\mathbf{E}^s = \frac{-2iab}{\lambda_0} (\hat{k}_i \cdot \hat{x}') \frac{\sin V}{V} \frac{\sin W}{W} \frac{e^{ik_o r}}{r} \mathbf{E}^i \tag{41}$$

where $W = k_0 a(\hat{k}_s \cdot \hat{y}')$ and V is given in (31).

VI. Modeling of a Corrugated Bark Layer

For some tree species, the bark layer is corrugated with grooves along the longitudinal direction. In this paper, the bark is simply modeled as a periodic corrugated layer with period L and width d as shown in Fig. 2(a). It is shown in [9] that,when $L < \lambda_0/2$ (single Bragg mode), the corrugated layer can be equivalently replaced by an anisotropic layer [see Fig. 2(b)] with the same thickness whose permittivity tensor

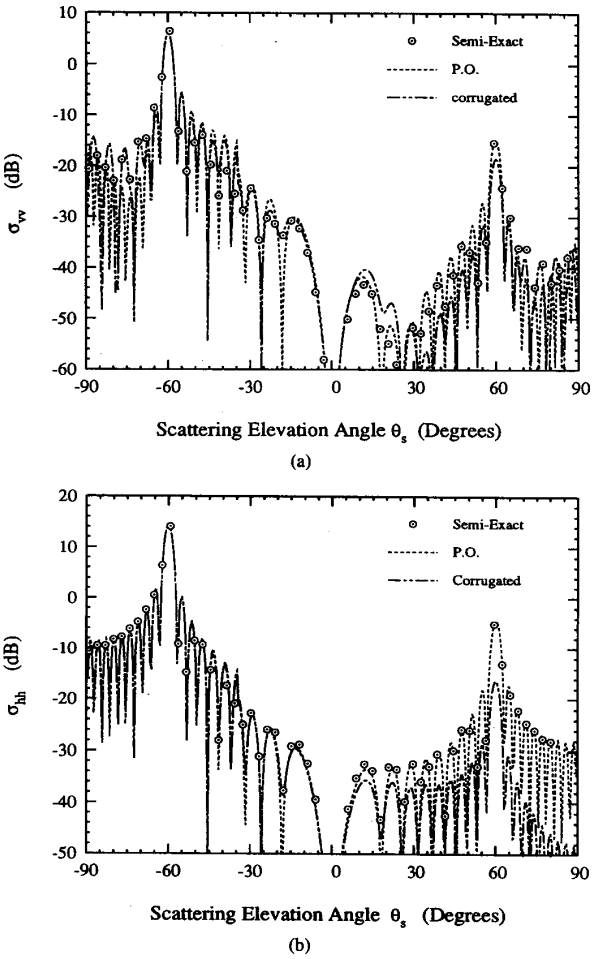

Fig. 5. The normalized bistatic (a) σ_{vv} and (b) σ_{hh} as a function of the scattering elevation angle θ_s in XZ-plane ($\theta_s > 0$ when $\phi_s = 0°; \theta_s < 0$ when $\phi_s = 180°$). The backscattered and the specular directions are shown at $\theta_s = 60°$ and $\theta_s = -60°$, respectively. Other parameters are $\theta_i = 120°$, $\phi_i = 180°$, $\theta_g = \theta_c = 0°$, $b = 20\lambda_0$, $a_1 = 2\lambda_0$, $a_2 = 1.8\lambda_0$.

is given by

$$\epsilon = \begin{pmatrix} \epsilon_{11} & 0 & 0 \\ 0 & \epsilon_{22} & 0 \\ 0 & 0 & \epsilon_{33} \end{pmatrix}. \tag{42}$$

The entries of the tensor in terms of the permittivity, period, and width of the corrugated layer, when $L \leq 0.2\lambda_0$, are approximated by

$$\epsilon_{11} = \frac{\epsilon_r}{\epsilon_r(1 - d/L) + d/L} \tag{43}$$

$$\epsilon_{22} = \epsilon_{33} = 1 + (\epsilon_r - 1)d/L. \tag{44}$$

Assuming that the radius of the cylinder is much larger than the wavelength, the permittivity of the bark layer can be represented by $\epsilon(\phi, z, n)$ where $\epsilon_{\phi\phi} = \epsilon_{11}$ and $\epsilon_{zz} = \epsilon_{nn} = \epsilon_{22}$.

To employ the PO approximation, a coordinate transformation from the local (ϕ, z, n) to (t, l, n) at SP point is needed. The resultant permittivity tensor in coordinate (t, l, n) is (45), (shown at the bottom of the page), where

$$\phi_z = \cos^{-1}\left[\frac{\hat{k}_i \cdot \hat{z}}{\sqrt{1 - (\hat{n} \cdot \hat{k}_i)^2}}\right]. \tag{46}$$

The reflected fields from a stratified anisotropic dielectric half space is computed using the method described in [13].

VII. Numerical Results

In this section a number of numerical examples for the scattering from a finite cylinder above a ground plane are presented. In all the considered examples the normalized RCS, defined by

$$\sigma_{pq} = \frac{4\pi|S_{pq}|^2}{k_0 ab^2} \tag{47}$$

are displayed for a two-layered cylinder with height b, exterior radius a_1 and interior radius a_2. The permittivity of the exterior and interior layers are chosen to be $\epsilon_1 = 4+i1$ and $\epsilon_2 = 10+i5$ respectively. Also the cylinder is positioned vertically ($\theta_c = 0$) on a tilted ground with permittivity $\epsilon_g = 10 + i5$.

First, the validity region of the PO approximation in the backscatter direction is examined. Fig. 3 compares σ_{vv} and σ_{hh} using the PO and semi-exact solutions. It is found that the PO solution agrees well with the semi-exact solution when $k_0 a > 10$. For small values of $k_0 a$ the resonance behavior of backscatter is shown by the semi-exact solution. Figs. 4–6 show the monostatic and bistatic scattering patterns which are simulated for a two-layered cylinder with and without a corrugation. The thickness of the corrugated layer and its filling factor are respectively chosen to be $t = 0.1\lambda_0$ and $d/L = 0.7$ (see Fig. 2). Fig. 4 shows the backscattering pattern as a function of incidence angle. At small angles of incidence, the PO approximation differs slightly from the semi-exact solution because the radial component of the propagation constant ($k_\rho = k_0 \sin\theta$) is small in this region and the condition $k_\rho a > 10$ is not satisfied. The vv-polarized backscattering RCS has two minima corresponding to the two Brewster angles one occurring on the surface of the cylinder ($\theta \simeq 25°$) and the other occurring on the ground plane ($\theta \simeq 75°$). The ripples on the curves are due to the components $\mathbf{S}_t$ and $\mathbf{S}_{gtg}$ (5), which become significant for angles of incidence close to 90°; and the oscillation rate is proportional to the cylinder length. This figure also shows the

$$\epsilon = \begin{pmatrix} \epsilon_{zz}\sin^2\phi_z + \epsilon_{\phi\phi}\cos^2\phi_z & (\epsilon_{\phi\phi} - \epsilon_{zz})\sin\phi_z\cos\phi_z & 0 \\ (\epsilon_{\phi\phi} - \epsilon_{zz})\sin\phi_z\cos\phi_z & \epsilon_{zz}\cos^2\phi_z + \epsilon_{\phi\phi}\sin^2\phi_z & 0 \\ 0 & 0 & \epsilon_{nn} \end{pmatrix} \tag{45}$$

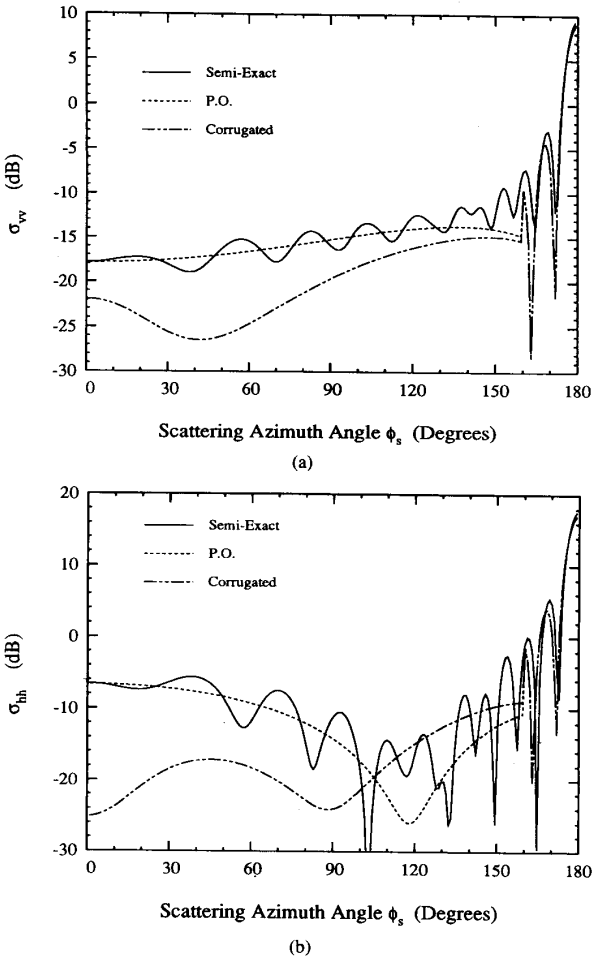

Fig. 6. The normalized bistatic (a) σ_{vv} and (b) σ_{hh} as a function of the scattering azimuth angle ϕ_s. The backscattered and forward-scattered direction are shown at $\phi_s = 0°$ and $\phi_s = 180°$, respectively. Other parameters are $\theta_i = 120°$, $\phi_i = 180°$, $\theta_s = 60°$, $\theta_g = \theta_c = 0°$, $b = 20\lambda_0$, $a_1 = 4\lambda_0$, $a_2 = 3.6\lambda_0$.

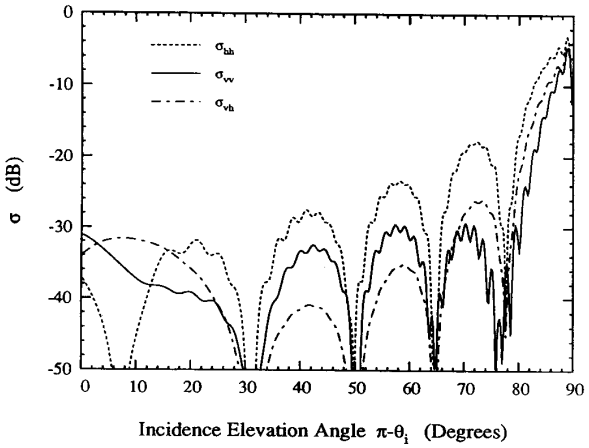

Fig. 7. The normalized backscattering RCS as a function of the incidence angle $\pi - \theta_i$ for a two layered cylinder above a tilted ground plane. Other parameters are $\theta_g = 20°$, $\phi_g = 90°$, $\theta_c = 0°$, $\phi_i = 180°$, $\phi_s = 0°$, $\theta_s = \pi - \theta_i$, $b = 20\lambda_0$, $a_1 = 2\lambda_0$, $a_2 = 1.8\lambda_0$.

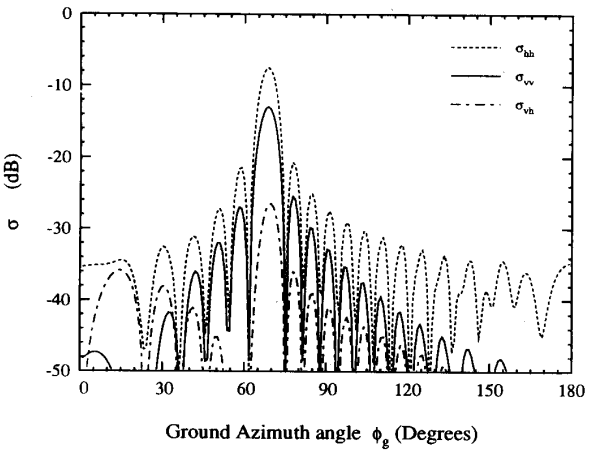

Fig. 8. The normalized backscattering RCS as a function of the ground azimuth angle ϕ_g. Other parameters are $\theta_g = 20°$, $\theta_c = 0°$, $\theta_i = 135°$,$\phi_i = 180°$, $\theta_s = 45°$, $\phi_s = 0°$, $b = 20\lambda_0$, $a_1 = 2\lambda_0$, $a_2 = 1.8\lambda_0$.

effect of the bark layer on the backscattering RCS. Depending on the incidence angle the RCS of the cylinder may be reduced as high as 10 dB. The reduction in the RCS is a function of the cylinder length and the corrugation parameters. Basically, the corrugated layer behaves as an impedance transformer between the air and the vegetation material. Fig. 5 shows the bistatic scattering pattern as a function of elevation angle when $\theta_i = 120°$, $\phi_i = 180°$ and the observation point is moving in the XZ-plane. Fig. 6 shows the bistatic scattering pattern as a function of azimuth angle (ϕ_s) with $\theta_i = 120°$, $\phi_i = 180°$, and $\theta_s = 60°$. The discontinuities found on the PO solution near the forward directions are because of switching the expression for scattering from (40) to (41).

Figs. 7–9 show the effect of the tilted ground plane on the backscattering RCS. All the parameters in Fig. 7 are the same as those given in Fig. 4 except for the tilt angle of the ground, $\theta_g = 20°$ and $\phi_g = 90°$. Comparing Fig. 4 with Fig. 7, it can be seen that a significant cross-polarized backscattered signal is generated due to the slope of the ground plane. Fig. 8 shows the variation of backscattering RCS as a function of the ground azimuth angle ϕ_g where $\theta_i = 135°$, $\phi_i = 180°$, and $\theta_g = 20°$. One can observe that the peak of the backscattering RCS occurs at $\phi_g = 70°(= \pi - \theta_g)$. Fig. 9 shows the backscattering RCS as a function of the ground elevation angle θ_g where $\theta_i = 135°$, $\phi_i = 180°$, and $\phi_g = 0°$ and 180°. The regions in the positive and the negative θ_g represent the ascending and the descending sides of a mountain respectively. In this case no cross-polarized signal is generated because the cylinder is in the principal plane (X–Z plane). Note that there are two maxima occurring at $\theta_g = 0°$ and $\theta_g = -22.5°$. The first maximum corresponds to the dihedral-like ground -trunk interaction. The second maximum corresponds to a reflection from the ground plane which illuminates the cylinder at normal incidence. The backscatter from the cylinder bounce off from the ground plane and returns toward the radar (see Fig. 10).

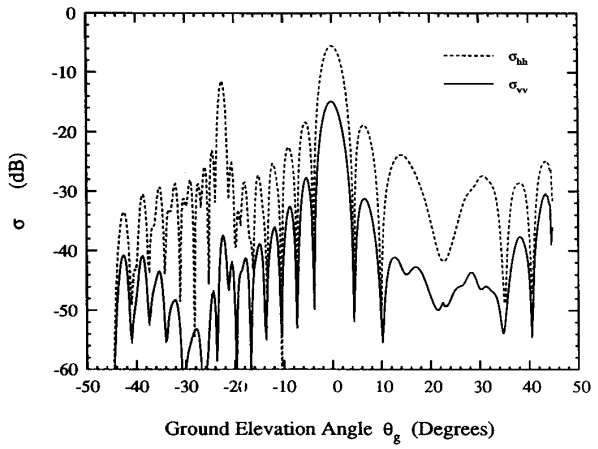

Fig. 9. The normalized backscattering RCS as a function of the ground elevation angle θ_g ($\theta_g > 0$ when $\phi_g = 0°$; $\theta_g < 0$ when $\phi_g = 180°$). Other parameters are $\theta_i = 135°$, $\phi_i = 180°$, $\theta_s = 45°$, $\phi_s = 0°$, $b = 20\lambda_0$, $a_1 = 2\lambda_0$, $a_2 = 1.8\lambda_0$.

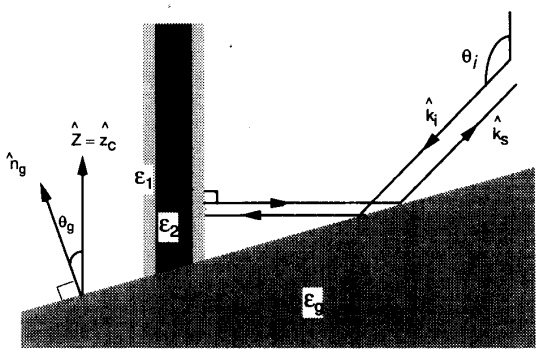

Fig. 10. The geometry of the scattering configurations for a cylinder over a tilted ground where a strong backscatter can be observed.

This strong backscatter component can be observed where $\hat{k}_i$, $\hat{n}_g$, and $\hat{z}_c$ are in the same plane and $\theta_i = 2\theta_g + \pi/2$.

VIII. Conclusions

An efficient and realistic electromagnetic scattering model for a tree trunk above a ground plane is presented in this paper. The trunk is modeled as a finite-length stratified dielectric cylinder with a corrugated bark layer. The ground is considered to be a smooth homogeneous dielectric with an arbitrary slope. An asymptotic solution based on the PO approximation for high frequencies is derived. This solution provides a fast algorithm with excellent accuracy when the radii of tree trunks are large compared to the wavelength. The effect of the bark layer is also taken into account by simply replacing the bark layer with an anisotropic layer. It is shown that the corrugated layer acts as an impedance transformer which may significantly decrease the backscattering RCS. The RCS reduction depends on the corrugation parameters. It is also shown that for a tilted ground plane a significant cross-polarized backscattered signal is generated while the co-polarized backscattered signal is reduced.

Acknowledgment

The authors would like to thank all the reviewers of this manuscript, whose comments helped to improve the quality of the final paper.

References

[1] F. T. Ulaby, K. Sarabandi, K. MacDonald, M. Whitt, and M. C. Dobson, "Michigan microwave canopy scattering model," *Int. J. Remote Sensing*, vol. 11, no. 7, pp. 1223–1253, 1990.

[2] L. Tsang, C. H. Chan, J. A. Kong, and J. Joseph, "Polarimetric signature of a canopy of dielectric cylinders based on first and second order vector radiative transfer theory," *J. Electromag. Waves and Appl.*, vol. 1, no. 1, pp. 19–51, 1992.

[3] S. L. Durden, J. J. van Zyl, and H. A. Zebker, "Modeling and observation of the radar polarization signature of forested areas," *IEEE Trans. Geosci. Remote Sensing*, vol. 27, pp. 290–301, May 1989.

[4] S. S. Seker and A. Schneider, "Electromagnetic scattering from a dielectric cylinder of finite length," *IEEE Trans. Antenna Propagat.*, vol. 36, no. 2, pp. 303–307, 1988.

[5] M. A. Karam and A. K. Fung, "Electromagnetic scattering from a layer of finite-length, randomly oriented dielectric circular cylinder over a rough interface with application to vegetation," *Int. J. Remote Sensing*, vol. 9, no. 6, pp. 1109–1134, 1988.

[6] F. T. Ulaby and C. Elachi, *Radar Polarimetry for Geoscience Applications*. Norwood, MA: Artech House, 1990.

[7] K. Sarabandi and F. T. Ulaby, "High frequency scattering from corrugated stratified cylinders," *IEEE Trans. Antennas Propagat.*, vol. 39, no. 4, pp. 512–520, 1991.

[8] K. Sarabandi, "Scattering from dielectric structures above impedance surfaces and resistive sheets," *IEEE Trans. Antennas Propagat.*, vol. 40, pp. 67–78, Jan. 1992.

[9] ——, "Simulation of a periodic dielectric corrugation with an equivalent anisotropic layer," *Int. J. Infrared Millimeter Waves*, vol. 11, pp. 1303–1321, 1990.

[10] J. J. van Zyl, "The effect of topography on radar scattering from vegetated areas," *IEEE Trans. Geosci. Remote Sensing*, vol. 31, pp. 153–160, Jan. 1993.

[11] G. T. Ruck, D. E. Barrick, W. D. Staurt, and C. K. Krichbaum, *Radar Cross Section Handbook*. New York: Plenum, 1970, pp. 259–263, 479–484.

[12] M. O. Kolawole, "Scattering from dielectric cylinders having radially layered permittivity," *J. Electromag. Waves Appl.*, vol. 16, no. 2, pp. 235–259, 1992.

[13] M. A. Morgan, "Electromagnetic scattering by stratified inhomogeneous anisotropic media," *IEEE Trans. Antennas Propagat.*, vol. AP-35, pp. 191–197, 1987.

[14] K. Sarabandi, "Electromagnetic scattering from vegetation canopies," Ph.D. dissertation, Univ. Michigan, Ann Arbor, 1989, pp. 224, eq. 7.40.

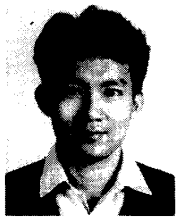

Yi-Cheng Lin (S'92) was born in Kaohsiung, Taiwan, in 1965. He received the B.S. degree in nuclear engineering from National Tsinghua University, Taiwan, and the M.S. degree in electrical engineering from National Taiwan University in 1987 and 1989, respectively. He is currently pursuing the Ph.D. degree at the University of Michigan, Ann Arbor.

Since Sept. 1993, he has been a Graduate Research Assistant at the University of Michigan Radiation Laboratory working in the area of microwave remote sensing. His main research interests include analytical and numerical techniques in scattering problems, near-field measurements and analysis, and microwave remote sensing of forest canopies.

Kamal Sarabandi (S'87–M'90–SM'93), for photograph and biography, please see p. 857 of this Transactions.